Numerical Analysis of Ultrashort Laser Ablation: Application for Fabrication of Nanoparticles and Nanostructures

M. E. Povarnitsyn, V. Fokin, A. Voloshko, L. Delfour, Tatiana Itina

▶ **To cite this version:**

M. E. Povarnitsyn, V. Fokin, A. Voloshko, L. Delfour, Tatiana Itina. Numerical Analysis of Ultrashort Laser Ablation: Application for Fabrication of Nanoparticles and Nanostructures . AIP Conference Proceedings, 2014, pp.8. ujm-01077430

HAL Id: ujm-01077430
https://ujm.hal.science/ujm-01077430

Submitted on 24 Oct 2014

HAL is a multi-disciplinary open access archive for the deposit and dissemination of scientific research documents, whether they are published or not. The documents may come from teaching and research institutions in France or abroad, or from public or private research centers.

L'archive ouverte pluridisciplinaire **HAL**, est destinée au dépôt et à la diffusion de documents scientifiques de niveau recherche, publiés ou non, émanant des établissements d'enseignement et de recherche français ou étrangers, des laboratoires publics ou privés.

Numerical Analysis of Ultrashort Laser Ablation: Application for Fabrication of Nanoparticles and Nanostructures

Mikhail Povarnitsyn[a], Vladimir Fokin[a], Andrey Voloshko[b], Laure Delfour[b], and Tatiana E. Itina[b]

[a] *Joint Institute for High Temperatures RAS, Izhorskaya 13 Bldg 2, 125412, Moscow, Russia.*
[b] *Hubert Curien Laboratory, UMR CNRS 5516/Lyon University, 18 rue Benoit Lauras, Bat. F, 42000, Saint-Etienne, France*

Abstract. In this study, first we examine nanoparticle formation by femtosecond laser ablation under different experimental conditions. The dynamics of the laser plume expansion is investigated and the possibility of primary nanoparticle formation is analyzed. Then, we consider thermalization process in a background environment, diffusion-driven nucleation and longer scale nanoparticle aggregation/sintering. In addition, laser-assisted fragmentation of nanoparticles is examined, which can play a particular role in the multi-pulse regime. In this later case, nanoparticle size distribution results from an ensemble of processes thus revealing different particle populations. Calculations are performed for metals under different background conditions. The calculation results explain recent experimental findings and help to predict the role of the experimental parameters. The obtained nanoparticles are also used to form nanostructures. The performed analysis thus indicates ways of a control over the involved laser-assisted techniques.

Keywords: Femtosecond laser, nanoparticle formation, modeling
PACS: 81, 81.16.Mk, 74.78.Na

INTRODUCTION

Ultrashort laser ablation is a unique tool for material nanostructuring and for nanoparticle synthesis [1,2]. This method provides possibilities of a very precise control over the laser processing. In particular, by using laser ablation, nanoparticles with a controlled size can be formed from different materials.

During last decade, numerous experiments have been performed, clearly demonstrating that in the case if femtosecond laser ablation, laser energy deposition induces an explosive ejection of a mixture of clusters and atoms [3,4,5,6,7,8] rather than an equilibrium surface evaporation. Despite a large number of the experimental results, the theoretical understanding of the physical and chemical mechanisms leading to the formation of nanoparticles during femtosecond laser ablation is still lacking.

To explain the experimentally observed processes, a number of analytical and numerical models have been proposed [9,10,11,12,3,13,14,15,16,17,18,19,20,21]. Two extreme cases of either very low or relatively high background pressure are considered in most theoretical studies of laser plume expansion. The plume expansion

into vacuum can be described as self-similar adiabatic one with condensation phenomenon [22,23,24,25,26,27]. In the case of high background pressure, shock waves were shown to be produced during the plume expansion into background gases [28]. To describe plume expansion, a system of Navier-Stocks equations was solved providing a wealth of information about the first 1-2 microseconds of the plasma plume expansion. Gas-dynamical models are, however, invalid if the velocity distribution of the ablated particles deviates from the Maxwellian distribution. These models also hardly describe inter-component mixing. As a result, they cannot be applied for delays longer than several microseconds. Therefore, in more recent studies [29], at 1-2 μs the hydrodynamic calculations were switched to the Direct Monte Carlo simulations where no such hypothesis is used.

To study femtosecond laser ablation, such approaches as molecular dynamics (MD), hydrodynamics (HD), and combinations with the direct simulation Monte Carlo method (DSMC) were proposed [30,31,32,33,34,35,36]. In particular, the MD-DSMC combination allows one to properly account for both the processes of cluster ejection and their following evolution during the laser plume expansion as a result of the gas-phase collisions.

Here, we focus our attention at the formation of metallic nanoparticles that have found many promising applications due to their unique plasmonic and chemical properties. When femtosecond lasers are used, these particles can be produced even vacuum. Nevertheless, very often either an ambient gas or a liquid is used in the modern nanoparticle synthesis techniques.

MODELING AND DISCUSSION

Nascent Ablation Plume and Primary Nanoparticle Ejection

To model laser energy absorption, phase transitions, as well as to investigate such affects as shock and rarefaction wave formation in the target, two major approaches were used: (i) molecular dynamics (MD) simulations; and (ii) two-temperature hydrodynamics (HD). Calculations performed with both of these numerical techniques (FIGURE 1) show that if ultra-short lasers interact with metallic targets, nanoparticles are formed and ejected at the very beginning of the nascent plume expansion. In particular, one can observe that upon a typical femtosecond laser interaction, the target material is decomposed in a mixture of gas and particles.

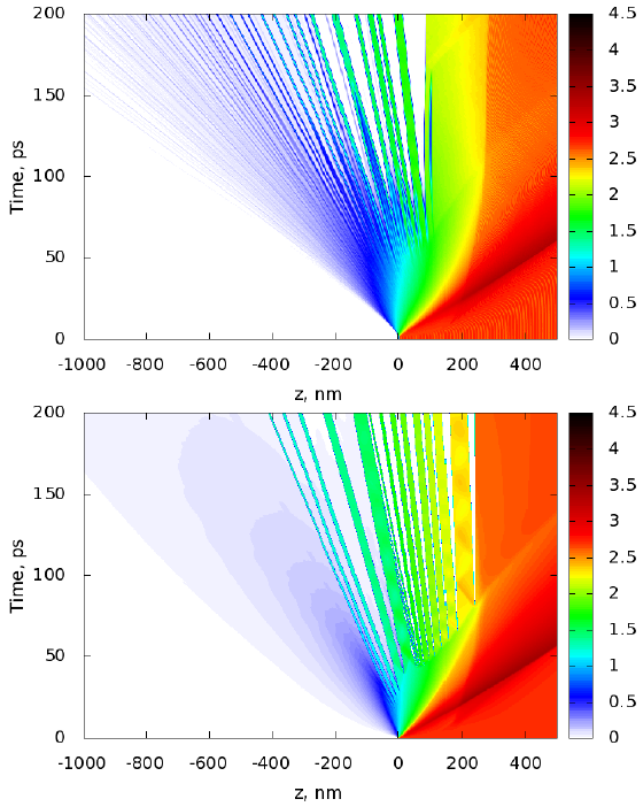

FIGURE 1 Femtosecond laser ablation of Cu. Here, density maps are obtained by (a) - MD and (b) - HD models, F= 2 J/cm^2

Despite a good agreement between the results obtained with MD and HD, there are several discrepancies that can be explained by the differences between the equation of state used in the HD calculations and the material properties obtained due to the interaction potential used in MD simulations.

The main advantage of the MD simulations is that there are no assumptions about thermodynamic equilibrium and no additional criteria are required to model phase explosion and material fragmentations. These effects appear as a result of the calculated dynamics of the ensemble of the considered atoms based on the employed interaction potential. Here, we use EAM potential of Zhakhovskii [37] that was verified in several papers by a comparison with the experiments [38]. In addition, MD simulations allow us to calculate particle size distribution and follow different plume populations. A decreasing function with two different slopes is typically obtained in the size distribution at such short delays [39]. We note that this distribution is modified by such effects as nucleation, condensation, coalescence/aggregation/sintering and/or fragmentation occur at longer delays. In what follows we will examine the role of these effects. For this, longer simulations should be performed.

Plume expansion: adiabatic expansion, plume stopping and thermalization. Nucleation in one component and two-component systems

As it was shown by both MD and HD calculations, the nascent femtosecond plume contains clusters and nanoparticles immediately after its formation, which should be taken into account in the plume expansion model. For this, we perform Direct Simulation Monte Carlo (DSMC) calculations of a metallic plume dynamics in the presence of an inert background gas (Ar). The initial conditions are defined by a parameterization of the corresponding MD calculations.

When ablation takes place in the presence of a background gas, the ablated material is compressed and part of it is scattered back. As a result, a typical mushroom-like shape is observed for atomic plume. This effect affects nanoparticles only slightly [40]. FIGUREs 2, 3 show typical calculation results obtained in the presence of a background gas. The spatial density distributions of atoms and clusters are shown separately for two different delays after the laser pulse. Here, larger clusters were initially at the back of the plume. The larger are the clusters the less pronounced is the stopping by the gas. These results are consistent with the experimental findings of Amoruso et al. [40].

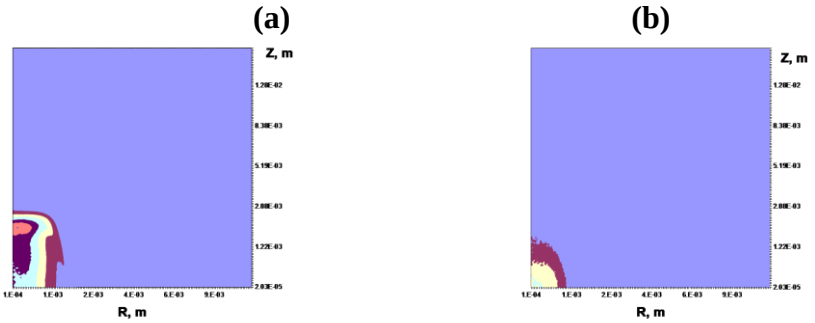

FIGURE 2. Calculated plume dynamics for the expansion in Ar gas at 300 Pa, (a) – density of atoms at t=0.55 μs, (b) –density of clusters at t=0.55 μs

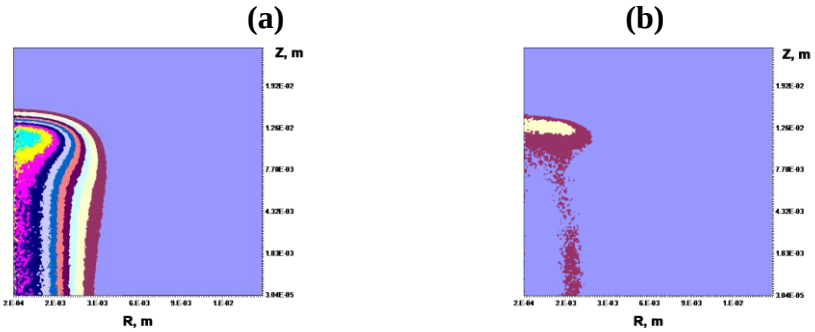

FIGURE 3. Calculated plume dynamics for the expansion in Ar gas at 300 Pa, (a) – density of atoms at t=10 μs, (b) –density of clusters at t=10 μs

The obtained results confirm that, for the given background pressure, plumes front starts experiencing a pronounced deceleration and practically stops at a certain delay (here, ~10μs). At the beginning, this effect is described by a so-called snow-plow model, then by the blast-wave (or, shock-wave) model, and at a later stage shock waves degenerate and, finally the plume species get thermalized and diffusion-driven

regime enters into play. In general, this effect starts when the mass of the adjacent background gas becomes comparable with the plume mass, or at a distance of [41]

$$L_f = \sqrt[3]{\frac{3}{2\pi}\frac{MkT_b}{m_b}}P_b^{-1/3}., \quad (1)$$

where M is plume mass; k is Boltzmann constant; P_b is the background pressure; T_b is temperature, and m_b is the atomic weight of background gas species. The estimation given by this equation is in good agreement with the calculated results shown in FIGURE 2.

The corresponding nanoparticle size distributions are shown in FIGURE 3. One can see that after a sufficient delay, a peaked distribution appears instead of the decreasing function.

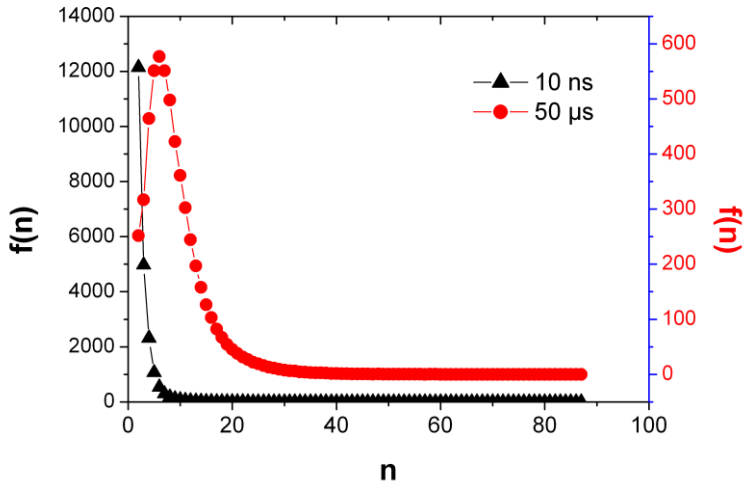

FIGURE 3. Size distributions calculated by using MD-DSMC model in the presence of 300 Pa of Ar

At distances shorter than L_f, plume expansion is free, and the metallic plume behaves as *one component gas* and can be described as an adiabatic process. If nucleation occurs, it is described by the supersaturating ratio, where saturation pressure is given by the Clausius–Clapeyron equation

$$\theta \approx 1 - \frac{T}{T_{eq}} = 1 - T\left\{\frac{1}{T_b} - \frac{k}{Q}\ln\left(\frac{P_{tot}}{P_b}\right)\right\}, \quad (2)$$

where $P_{tot} = P$ is metallic vapor pressure in the case of one-component adiabatic expansion; and Q is the vaporization heat. Typical estimation results obtained by using these equations are presented in [35]. These estimations are valid only until the delay determined by the beginning of the efficient mixing between the plume and ambient species (t~1-10 μs).

For a considerable nucleation to occur, plume temperature should drop rapidly. Roughly, one can use the following estimation: $c_p T < Q$, where C_p is the metal vapor heat capacity. This condition gives T~500 K for Au and ~670 K for Ni. During femtosecond ablation in the presence of a background gas, such plume temperatures are achieved only at the plume thermalization stage. Upon both mixing and thermalization process, the stopping distance of the plume ions and atoms is approximately estimated as follows [42]

$$L = \frac{kT_b}{\sqrt{2}\sigma_{ab} P_b}. \quad (3)$$

where the collision cross section $\sigma_{ab} \approx 10^{-15}$ cm^2. For P_b=300 Pa and T_b=300K, the typical stopping length L~10^{-2} cm. The total distance L_{tot}~L_f+L is typically reached by the delay of 1-5 μs. Starting from this time, nucleation mostly takes place in the *two-component* mixture, so that P_{tot}=P+P_b in Eq. 2. If the background pressure is high enough, this effect bursts nucleation since saturation is reached much faster. As a result, diffusion-driven nanoparticle formation prevails. We consider this process in the next section.

Diffusion-driven Nanoparticle Formation: Different Populations

In the presence of a background environment, diffusion-driven nucleation and aggregation processes take place. The firsts process leads to the formation of small nanoclusters (n-monomer nucleus), whose size is controlled by the free energy as follows

$$\Delta G(n,c) = -nkT \ln(c/c_0) + 4\pi a^2 n^{2/3} \sigma, \quad (4)$$

where k is the Boltzmann constant; T is the temperature in Kelvins; a is the effective radius; c_0 is the equilibrium concentration of monomers; and σ is the effective surface tension. The peak of the nucleation barrier corresponds to the critical cluster size

$$n_c = \left[\frac{8\pi a^2 \sigma}{3kT \ln(c/c_0)} \right]^3 \quad (5)$$

The production rate of supercritical clusters is then given by

$$\rho(t) = K_c c^2 \exp\left[\frac{-\Delta G(n_c, c)}{kT} \right], \quad (6)$$

$$K_n = 4\pi\left(a + an^{1/3}\right)\left(D_a + D_a n^{-1/3}\right) \approx 4\pi a n^{1/3} D_a, \quad (7)$$

and the evolution of the singlet population is given by

$$\frac{dN_1}{dt} = \rho(t) - \sum_{j=2}^{\infty} j \frac{dN_j}{dt}, \tag{8}$$

and for s=2 the master equation is

$$\frac{dN_2}{dt} = fK_1 N_1^2 - K_2 N_1 N_2, \tag{9}$$

where f is the kinetic parameter. As a result, very narrow size distributions can be produced [43]. The cluster time-evolution can be described by a simplified master equation of Smoluchowski [43]

$$\frac{dN}{dt} = K_{S-1} N_1 N_{S-1} - K_S N_1 N_S \ (s \geq 3), \tag{10}$$

where $N_s(t)$ is the time-dependent number density of the secondary particles containing s primary particles; $K_s = 4\pi(R_1 + R_s)(D_1 + D_S)$ is the attachment rate constant; $R_s = 1.2rs^{1/3}$; r is the average radius of the primary particle; $D_s = D_1 s^{-1/3}$ is the diffusion coefficient. In addition, in part of the presented calculations we include laser-induced nanoparticle fragmentation [44].

A series of calculations are performed with parameters typical for femtosecond laser ablation of gold. Calculation parameters are similar to that in Ref. 43.

The obtained results (FIGURE 5) clearly show that the peak is due to the nucleation process that provides critical sized clusters.

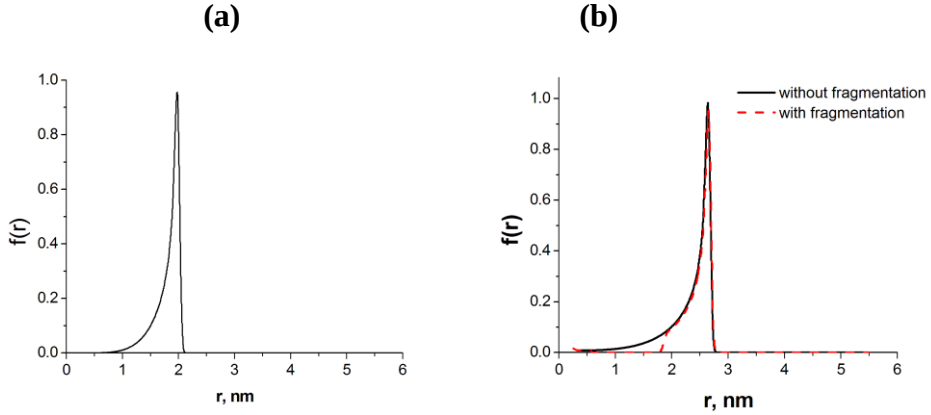

FIGURE 5. Calculated size distribution obtained in calculations (a) – for a single pulse without fragmentation (t=0.1 s); and (b) – for 10 pulses with and without fragmentation. Here, gold solution in water is considered a=1.59^{-10}, other calculation parameters are given in [43].

These small nuclei then grow due to the aggregation process shifting the distribution to the right, but the narrow peak can be still observed even at a quit long delay. In addition, we include a possibility of laser-assisted nanoparticle fragmentation. One can see in the FIGURE that when several pulses are applied, nanoparticle distribution

is shifted to the right because there is more ablated material. Fragmentation can create a hole in the distribution and can separate different particle populations (FIGURE 5b).

SUMMARY

Calculation results are presented for femtosecond laser interactions. We have considered several mechanisms of nanoparticle formation. he performed calculations have demonstrated the following

(i) Primary particles are mostly ejected from the metastable liquid phase. Part of them is also formed by nucleation.

(ii) Longer evolution in the background gas or a liquid involves nucleation, growth and fragmentation thus providing a possibility for the formation of several populations.

We note, finally, that the produced nanoparticles can be deposited on a substrate and form nanostructures. Therefore, the presented study is of interest for many applications connected with both metallic nanoparticles and nanostructures.

ACKNOWLEDGMENTS

We gratefully acknowledge supports from the CNRS of France (PICS 6106 France-Russia project, CINES x2014085015) and from the Russian Foundation for Basic Research (project nos. 13-08-01179 and 13-02-91057).

REFERENCES

[1] T. E. Itina, N. Bouflous, J. Hermann, P. Delaporte, SPIE Proceedings 2011, 8414.
[2] M. E. Povarnitsyn, T.E. Itina, M. Sentis, P. Levashov, K. V. Khishchenko, Phys. Rev. B. **75**, 235414 (2007).
[3] L. V. Zhigilei, B. J. Garrison, J. Appl. Phys. 88, (3), 1281, (2000)
[4] M. E. Povarnitsyn, T. E. Itina, M. Sentis, K. V. Khishenko, P. R. Levashov, Phys. Rev. B , 75, 235414 (2007)
[5] A. V. Bulgakov, I. Ozerov, W. Marine, Appl. Phys. A 79, 1591 (2004).
[6] S. Amoruso, R. Bruzzese, N. Spinelli, R. Velotta, M. Vitello, and X. Wang, Europhys. Lett. 67, 404 (2004).
[7] M.E. Povarnitsyn, N.E. Andreev, E.M. Apfelbaum, T. E. Itina, K.V. Khishchenko, O.F. Kostenko, P. R. Levashov, M. Veysmann, Appl. Surf. Sci. 258(23) , 9480-9483 (2012)
[8] S. Amoruso, R. Bruzzese, M. Vitiello, N. N. Nedialkov, and P. A. Atanasov, J. Appl. Phys. 98, 044907 (2005).
[9] S.I. Anisimov, D. Bäuerly and B.S. Luk'yanchuk, Phys. Rev. B 48, (1993) 12076.
[10] K.L. Saenger: J. Appl. Phys. 70(10) (1991) 5629.
[11] R. Kelly and R.W. Dreyfus: Nucl. Instrum. Meth. B32 (1988) 314.
[12] D. Sibold and H.M. Urbassek: Phys. Rev. A 43 (1991) 6722.
[13] T.E. Itina, A.A. Katassonov, W. Marine, and M. Autric: J. Appl. Phys. 83(11) (1998) 6050.
[14] T.E. Itina, W. Marine, M. Autric: J. Appl. Phys. 92(7) (1997) 3536.
[15] T.E. Itina, V. Tokarev, W. Marine, M. Autric: J. Chem. Phys. 106(21) (1997) 8905.
[16] T.E. Itina, L. Patrone, W. Marine, M. Autric: Appl. Phys. A69 (1999) S59.

[17] A.D. Akhsakhalyan, S.V. Gaponov, V.I. Luchin and A.P. Chirimanov: Sov. Phys. Tech. Phys. 33 (1988) 1885.
[18] N. Arnold, J. Gruber and J. Heitz: Appl. Phys. A. 69(7) (1999) S87.
[19] J.N. Leboef, K.R. Chen, J.M. Donato, D.B. Geohegan, C.L. Liu, A.A. Puretzky, and R.F. Wood: Phys. Plasmas 3(5) (1996) 2203
[20] J.N. Leboeuf, R.F. Wood, R.K. Chen, A.A. Puretzky, D.B. Geohegan: Phys. Rev. Lett. 79(8) (1997) 1571.
[21] H.C. Le, D.E. Zeitoun, J.D. Parisse, M. Sentis, W. Marine: Phys. Rev. E. 62(3) (2000) 4152.
[22] S. I. Anisimov, Zh. Eksp. Teor. Fiz. 54, 339 (1968) [Sov. Phys. JETP, 27, 182 (1968)].
[23] A. V. Bulgakov and N. M. Bulgakova, J. Phys. D: Appl. Phys. 28, 1710 (1995).
[24] Y. B. Zeldovich, Yu. P. Raizer, Physics of Shock Waves and High Temperature Hydrodynamic Phenomena (Academic Press, London, 1966).
[25] B. Luk'yanchuk, W. Marine, and S. Anisimov, Laser Phys. 8, 291 (1998).
[26] A. V. Gusarov, A. V. Gnedovets, and I. Smurov, J. Appl. Phys. 88, 4362 (2000).
[27] T. Ohkubo, M. Kuwata, B. Luk'yanchuk, T. Yabe, Appl. Phys. A. 77, 271 (2003).
[28] L.I. Sedov: Similarity and Dimensional Methods in Mechanics, Academic Press, London, 1959.
[29] T.E. Itina, J. Hermann, P. Delaporte, M. Sentis, Phys. Rev. E, 66, 066406 (2002).
[30] G. A. Bird, Molecular Gas Dynamics and the Direct Simulation of Gas Flows (Clarendon, Oxford, 1994).
[31] T.E. Itina, J. Hermann, P. Delaporte, M. Sentis, Phys. Rev. E, 66, 066406 (2002).
[32] T. E. Itina, K. Gouriet, L. V. Zhigilei, S. Noel, J. Hermann, and M. Sentis, Appl. Surf. Sci. , 253, 7656-7661 (2007)
[33] T. E. Itina, N. Bouflous, J. Hermann, P. Delaporte, SPIE Proc., 8414**,** DOI**:** 10.1117 /12.923129 (2011).
[34] T. E. Itina, K. Gouriet, L. V. Zhigilei, S. Noel, J. Hermann, and M. Sentis, Appl. Surf. Sci. , 253, 7656-7661, (2007)
[35] T. E. Itina and A. Voloshko, Appl. Phys. B, DOI: 10.1007/s00340-013-5490-6 (2013)
[36] T. E. Itina, J. Phys. Chem. C 115 (12), 5044, (2011)
[37] V. Zhakhovskii, N. Inogamov, Y. Petrov, S. Ashitkov, and K. Nishihara, Appl. Surf. Sci. 255, 9592–9596 (2009).
[38] 39 M. Hashida, A. Semerok, O. Goberta, G. Petiteb, and J.-F. Wagner, SPIE Proceedings, 2001, 4423, pp. 178–185.
[39] C. Wu and L. V. Zhigilei, , Appl. Phys. A 2014, 114, pp11-32.
[40] S. Amoruso, R. Bruzzese, X. Wang, and J. Xia, Appl. Phys. Lett. 93, 191504 (2008).
[41] S. Amoruso, B. Toftmann, J. Schou, Phys. Rev. E 69, 056403 (2004)
[42] M. R . Rashidian Vaziri, F Hajiesmaeilbaigi and M H Maleki, J. Phys. D: Appl. Phys. 43 (2010) 425205
[43]. J. Park, V. Privman, E. Matijevic, J. Chem. Phys. B 105, 11603-11635 (2001) .
[44] R. R Letfullin, Ch. Joenathan, Th. F George , V. P Zharov, Nanomedicine 2006, Vol. 1, No. 4, pp 473-480